CLASSIFICATION OF POLARIMETRIC SAR IMAGES BASED ON SCATTERING MECHANISMS

M. Ouarzeddine*, B. Souissi, A. Belhadj-Aissa

Université des Sciences et de la technologie Houari Boumedienne, Faculté d'électronique et d'informatique, BP N°32, El Alia, Alger, Algérie- (m.ouarzeddine@lycos.com, souissib@hotmail.com, h.belhadj@lycos.com)

KEY WORDS: Classification, polarimetry, decomposition, Pauli, polarimetric response, scattering

ABSTRACT:

Polarimetric classification is one of the most significant applications of polarimetric radar in remote sensing. During the last decade, several research tasks revealed the contribution of polarimetric data in classification of soil types and landcover. They contributed thus to a better comprehension of the scattering mechanisms. We propose in this paper a strategy analysis for forest types discrimination and their cartography on the ground using fully polarimetric data based on scattering matrix decompositions. To determine the scattering mechanism associated to each pixel with the target, we developed a supervised classification procedure where the training set is established from the entropy/Alpha space. The polarimetric coherence matrix was used to determine soil scattering parameters. To this end, we described two scattering types: deterministic scattering and random scattering. Classification of the image gives good discrimination of forests types and the results are checked using polarimetric signatures. The test area used is the Oberpfaffenhofen in Munich. The SAR images are acquired in the P band.

RESUME:

La classification polarimétrique est l'une des applications les plus importante de la polarimétrie radar en télédétection. Durant la dernière décennie, plusieurs travaux de recherche ont montré la contribution des données polarimétriques en classification des types de sols et les types de couverts de sol. Ainsi, ils ont contribué à une meilleure compréhension des mécanismes de diffusion. Nous proposons dans cette article une stratégie d'analyse pour la discrimination des types de forets et leur cartographie sur le sol, en utilisant des données radar complètement polarimétrique basé sur la décomposition de la matrice de diffusion. Pour déterminer le mécanisme de diffusion associé à chaque pixel avec la cible, nous avons développé une classification supervisée, ou la base d'entraînement est établit à partir de l'espace entropie/Alpha. La matrice polarimétrique de cohérence a été utilisée pour déterminer les paramètres de diffusion du sol.
Dans ce but, nous décrivons deux types de diffusion : Diffusion déterministe et diffusion aléatoire. La classification de l'image donne une bonne discrimination des types de forêts et les résultas sont vérifiées en utilisant les signatures polarimétriques. Le site d'étude est la zone de Oberpfafenhoffen à Munich. Les images RSO sont acquises dans la bande P.

1. INTRODUCTION

Conventional imaging radars operate with single fixed polarisation antenna for both transmission and reception. A unique backscattering coefficient is measured for a given resolution cell. Classification of SAR data acquired in single polarisation is difficult because of the poor separability of different characteristic scatters at the ground. None scattering dependence is gained with conventional radars. The availability of different polarisations is necessary (Evans et *al.,* 1988), hence these can lead to the improvement of radar detection when the behaviour of the parameters related to the objects on the ground is not identical.
Throughout the years and especially in the last two decades, the ability of radar polarimetry to obtain more information about physical properties of the surface than single-channel SAR data has led to a wide range of applications in geoscientific research in agriculture and in particular, forests have both a fundamental economic and environmental role. In this way, several investigations have reported the use of polarmetric data to map the forests types (Proisy et *al.*, 2002, Freeman & Durden, 1998).
Polarimetric data allows a better characterisation of the scatters based on decomposition theorems (Cloude & Pottier, 1996). Several works were focused on these theorems to identify the scattering mechanisms and their properties.
In this paper, We propose an analysis and classification of fully polarimetric data acquired on a forested area using a combination of entropy/alpha/anisotropy and complex Wishart classifier. A retrieval of forests types characteristics polarimetric signatures is also calculated, studied and analysed.

2. DATA USED

The data is the site of obepfaffenhofen procured in May 2000 covering the southern part of Munich, Germany and an area that embraces about 1 Km^2 was chosen in this study. The radar is the Aeos1 of the Ex private Aerosensing GmBH company. An airborne radar with the P band (72 cm).
The SAR images are acquired in fully polarimetric mode and are important value to supply information on the terrain type.
Figure 1 shows a 3D colour composite of the test site using the Pauli basis. This is just one of many possible ways to display a polarimetric SAR data.

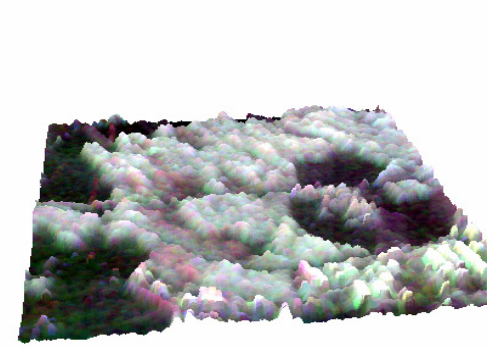

Figure 1: RGB 3D view of the test site in the Pauli basis

The P band wavelength is able to penetrate the forest canopy and hence offers the possibility to obtain information on the phase and on the amplitude of the scattered signal on the ground.
We give also in figure 2 , the identification of forest classes based on visual interpretation. On this image, we distinguish four types of forests :
Class 1: Mixed natural young forest: Very young (bout 4-5 years old), both coniferous and deciduous dense trees are contained in this forest class.
Class 2: Dense coniferous forest This class of forest contains coniferous trees, which are relatively higher (in average 30m)and are so dense.
Class 3: Old deciduous forest: This forest class contains old deciduous trees. They have big stem and medium height (20m)Trees are populated with low dense.
Class 4: Young deciduous forest: This class contains both coniferous and young deciduous trees . Both trees are in medium size and have medium dense population. Trees height have an average 15m.

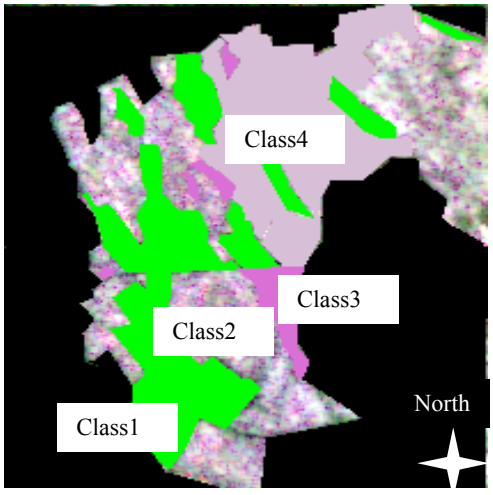

Figure 2: Identification of forest classes

3. POLARIMETRIC DATA ANALYSIS

3.1 Scattering matrix vectorisation

The scattering behaviour of canonical scatters can be described by a single constant scattering matrix S. In real ground environment, it is rare that one encounters such components. The assumption of canonical scatters is not valid because the received signal by the SAR system for a resolution cell is the result of many spatially distributed elementary scattering. We talk then about a distributed target. Each individual element is characterised by an individual scatters. The distributed target is characterised by the coherent superposition of the elementary scattering matrices.
Polarimetric decompositions rely on the scattering matrix which describes mainly how radar targets or the elements on the ground surface scatter the electromagnetic energy. This matrix which is of (2x2) dimension is built for each Pixel. It is defined by (Ulaby and Elachi, 1990):

$$S = \begin{pmatrix} S_{HH} & S_{HV} \\ S_{VH} & S_{VV} \end{pmatrix} \quad (1)$$

In radar polarimetry, scattering matrix is transformed into vector format in order to achieve decompositions.

3.2 Decomposition theorems

The first objective of decomposition theory is to express the average of the scattering mechanism in the resolution cell in a sum of independent elements aiming to associate a physical mechanism to each type of scattering (Cloude & Pottier).
Several decomposition techniques ere proposed. These techniques are based on three principal approaches (Touzi & Chabonneau, 2002) methods, Huynen decomposition and non coherent methods. These methods split the scattering matrix into the sum of elementary scattering matrices, each one defining a deterministic scattering mechanism. Two essential basis are used in the literature: the Pauli basis and the lexicographic basis.
The Pauli vector is given by:

$$\vec{K}_p = \frac{1}{\sqrt{2}} \begin{bmatrix} S_{hh} + S_{vv} \\ S_{hh} - S_{vv} \\ 2S_{hv} \end{bmatrix} \quad (2)$$

The first element of the vector is assigned to odd bounce scatterer such as the sphere, the plane surface or reflectors of trihedral type. The second one is related to a dihedral scatters or double isotropic bounce and the third element is related to horizontal and a cross polarising associated to the diffuse scattering or the volume scattering. In general, the polarimetric response of a given pixel is often a result of a mixture of scattering mechanisms.

In this work we are using the non coherent decomposition proposed by Cloude and Pottier using the Pauli basis. It is based on the coherency matrix formed by (Cloude and Pottier, 1997):

$$[T] = \left\langle \vec{k}_p . \vec{k}_p^{T} \right\rangle \quad (3)$$

This is a multilook 3x3 positive semi-definite hermitian coherency matrix where the superscript T denotes the matrix transpose, and $< >$ indicates multilook averaging. The $\sqrt{2}$ on the term is to ensure consistency in the span (total power) computation.

The eigenvectors and eigenvalues of the coherency matrix $\langle [T] \rangle$ can be calculated to generate a diagonal form of the coherency matrix which can be physically interpreted as statistical independence between a set of target vectors.

The eigenvalues of $\langle [T] \rangle$ therefore have direct physical significance in terms of the components of scattered power into a set of orthogonal unitary scattering mechanisms given by the eigenvectors of $\langle [T] \rangle$, which for radar backscatter themselves form the columns of a 3 x 3 unitary matrix. Hence we can write an arbitrary coherency matrix in the form (Papathanassiou, 1999):

$$\langle [T] \rangle = [U_3][\Sigma][U_3]^{-1} = \sum_{i=1}^{i=3} \lambda_i u_i u_i^{*T} \quad (4)$$

where $[\Sigma]$ is a 3x3 diagonal matrix with nonnegative real elements

$$[\Sigma] = \begin{bmatrix} \lambda_1 & 0 & 0 \\ 0 & \lambda_2 & 0 \\ 0 & 0 & \lambda_3 \end{bmatrix} \quad (5)$$

and $[U_3] = [u_1 \quad u_2 \quad u_3]$ is a unitary matrix given by:

$$[U_3] = \begin{bmatrix} \cos\alpha_1 & \cos\alpha_2 & \cos\alpha_3 \\ \sin\alpha_1 \cos\beta_1 e^{i\delta_1} & \sin\alpha_2 \cos\beta_2 e^{i\delta_2} & \sin\alpha_3 \cos\beta_3 e^{i\delta_3} \\ \sin\alpha_1 \sin\beta_1 e^{i\gamma_1} & \sin\alpha_2 \sin\beta_2 e^{i\gamma_2} & \sin\alpha_3 \sin\beta_3 e^{i\gamma_3} \end{bmatrix} \quad (6)$$

where u_1, u_2, and u_3 are the three unit orthogonal eigenvectors.

There are four variables of interest, two from the eigenvalues, namely the entropy H and anisotropy A, and two from the eigenvectors, the α and β angles. The parameter α is an indicator of the type of scattering mechanism, and it ranges from 0 to 90 degrees. These parameters are easily evaluated as (Cloude & Pottier):

$$\alpha = \sum_{i=1}^{i=3} P_i \alpha_i \quad (7)$$

P_i are the probabilities obtained from the eigenvalues λ_i :

$$0 \le P_i = \frac{\lambda_i}{\sum_{i=1}^{i=3} \lambda_i} \le 1 \quad (8)$$

To introduce the degree of statistical disorder of each target, the entropy is defined from the logarithmic sum of eigenvalues of the coherency matrix as :

$$H = -\sum_{i=1}^{i=3} P_i \log_3(P_i) \quad (9)$$

The entropy H represents the randomness of the scattering. H = 0 indicates a single scattering mechanism (isotropic scattering) while H = 1 indicates a random mixture of scattering mechanisms with equal probability and hence a depolarising target.

The anisotropy A is a parameter complementary to the entropy. The anisotropy measures the relative scattering of the second and the third eigenvalues of the eigen-decomposition. It is given by:

$$A = \frac{\lambda_2 - \lambda_3}{\lambda_2 + \lambda_3} \quad (10)$$

3.3 Entropy/Alpha space

analysis was carried out to study the behaviour of the principal forest types on the study site and to investigate the polarimetric parameters extracted from SAR data in order to discriminate the observed classes. The parameters chosen correspond to parameters frequently used in the literature: backscattering coefficients, entropy, α-angle, and anisotropy.

If the pair $H - \alpha$ plotted on a plane then they are confined to a finite zone as shown in figure 3. This plane is subdivided into eight zones characterising different classes of different scattering mechanisms, (alpha angle is evaluated in degrees).

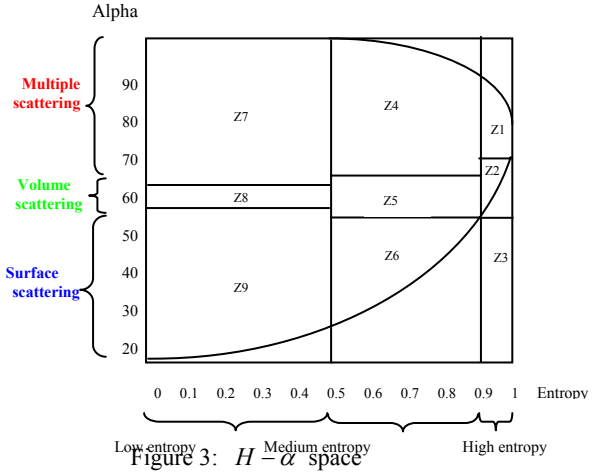

Figure 3: $H - \alpha$ space

3.4 Combined Wishart classifier

When the anisotropy parameter is introduced , it allows the possibility to distinguish different clusters where the centres

belong to the same $H-\overline{\alpha}$ partition. Each zone in the H/α space is splited in two. This technique increases the number of classes from 8 to 16 taking into account the secondary scattering.

With the introduction of the anisotropy, more details can be observed.

The eight and the sixteen classes resulted from the $H-\overline{\alpha}$ and $H/A/\overline{\alpha}$ decompositions are used as training sets for the initialisation of the unsupervised Wishart classifier (Lee et *al.*, 1999).

For a coherency matrix $\langle T_i \rangle$ of a pixel i of a multilook image (L-looks) knowing the class ωi, the Wishart complex distribution is given by:

$$p(\langle T_i \rangle / \omega_m) = \frac{N^{qN} \left|\langle T_i \rangle\right|^{N-q} \exp(-tr(N[\Sigma_m]^{-1}\langle T_i \rangle))}{K(N,q)\left|\Sigma_m\right|^N} \tag{11}$$

With

$$\Sigma_m = E\left(\langle T_i \rangle \middle| \langle T_i \rangle \in \omega_m\right) \tag{12}$$

$$= \frac{1}{N_m}\sum_{i=1}^{N_m}\langle T_i \rangle \tag{13}$$

Where *Nm* is the pixels number of *wm*

And $K(N,q)$ is the factor of standardisation given by

$$K(N,q) = \pi^{q(q-1)/2}\prod_{i=1}^{q}\Gamma(N-i+1) \tag{14}$$

Where q=3 in the case of reciprocity (i.e., Shv=Svh), $|\ |$ and tr (.) indicate the determinant and the trace of the matrix respectively, and $\Gamma(.)$ is the gamma function.

A probabilistic measurement of the distance between the matrix of coherence of an unspecified pixel $\langle T_i \rangle$, and the average matrix of coherence Σ_m of the class candidate wm, is obtained using:

$$d(\langle [T_i] \rangle, \Sigma_m) = \ln\left|\Sigma_m\right| + tr(\Sigma_m^{-1}\langle [T_i] \rangle) \tag{15}$$

Mathematically, each coherency matrix of an individual pixel is assigned with the most likely class ω_m with the minimal distance, if and only if :

$$d(\langle [T_i] \rangle, \Sigma_m) \le d(\langle [T_i] \rangle, \Sigma_n) \tag{16}$$

for all $w_m \neq w_n$

The result of the combined entropy/anisotropy/alpha decomposition with the complex Wishart distribution is given in Figure 4.

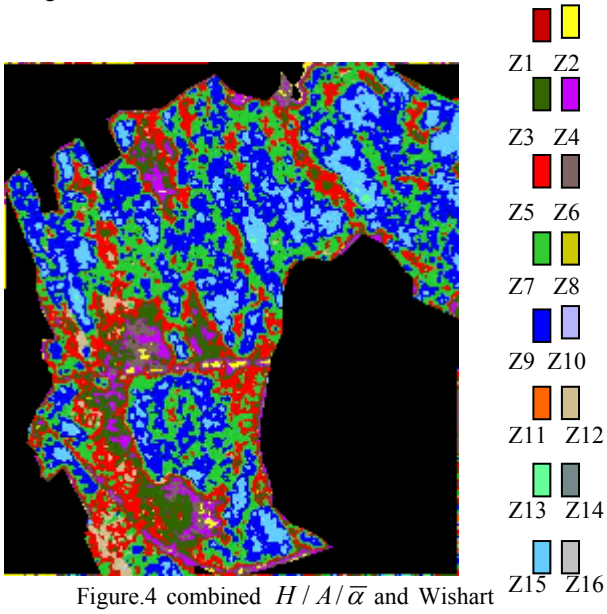

Figure.4 combined $H/A/\overline{\alpha}$ and Wishart classied image

In the $H/A/\overline{\alpha}$ decomposition, The Z1, Z3, Z5, Z7, Z9, Z11, Z13, Z15 are weak anisotropy zones (A less then 0.5) and Z2, Z4, Z6, Z8, Z10, Z12, Z14, Z16 (A bigger then 0.5) are zones with important degree of anisotropy. For the creation of forest map, the H/α/A parameters alone do not provide a sufficient information, therefore an extended unsupervised combined Wishart classifier is proposed in order to best extract physical information and distinguish between different forest classes (Figure 4). The results obtained from the combined classification show that the P-band provides discrimination capability. We observe four forest classes with different degrees of scattering mechanisms due to their structural parameters. If we compare this result to the classified reference image based on visual interpretation, we find it different. This is because of the nature of the classification method which is unsupervised. The mixed natural young forest was classified as having volume scattering with high entropy and multiple scattering approaching more the nature of a dense field because of the presence of shrubs. The major scattering mechanisms of the dense forest belongs to the type of medium entropy surface scattering, this is because of the dominance of needles, brunches and trunks whilst the old deciduous forest shows medium entropy multiple scattering, the reason is the leaves which are larger then of those found with coniferous forest and hence the scattering is higher. For the young deciduous forest, the dominant scattering has a medium entropy and it includes the basic types of the scattering mechanisms. This characterisation is endorsed with polarimetric responses.

3.5 Polarimetric response

3.5.1 Theoretical background

Polarisation synthesis can also be expressed in terms of the Muller matrix M (Ulaby and Elachi, 1990). M is a 4x4 symmetrical matrix, whose elements are all real.

$$[M] = [\tilde{R}]^{-1} [W][R]^{-1} \quad (17)$$

where

$$R = \begin{bmatrix} 1 & 1 & 0 & 0 \\ 1 & -1 & 0 & 0 \\ 0 & 0 & 1 & 1 \\ 0 & 0 & -i & i \end{bmatrix} \quad (18)$$

and

$$W = \begin{bmatrix} s_{vv}s_{vv}^* & s_{vh}s_{vh}^* & s_{vh}s_{vv}^* & s_{vv}s_{vh}^* \\ s_{hv}s_{hv}^* & s_{hh}s_{hh}^* & s_{hh}s_{hv}^* & s_{hv}s_{hh}^* \\ s_{hv}s_{vv}^* & s_{hh}s_{vh}^* & s_{hh}s_{vv}^* & s_{hv}s_{vh}^* \\ s_{vv}s_{hv}^* & s_{vh}s_{hh}^* & s_{vh}s_{hv}^* & s_{vv}s_{hh}^* \end{bmatrix} \quad (19)$$

$[\tilde{R}]$ means the transpose of the matrix $[R]$ and the asterisk denotes complex conjugation.

The backscattering radar cross section (RCS) characterises the backscattering property of an illuminated target by an electromagnetic waves, and depends on its size, shapes, and orientation as well as on wavelength and polarisation of the incident signal.

Finally, the backscattering cross section σ was calculated for both the co-pol and cross-pol scattering cases. These equations allowed the cross sections to be computed for many types of surfaces. For the co-pol , σ is determined for any arbitrary polarisation state by calculating the Muller matrix M and the transmit and receive Stokes vectors.

$$\sigma(\chi,\psi) = \frac{4\pi}{k^2} \begin{bmatrix} 1 \\ \cos 2\chi \cos 2\psi \\ \cos 2\chi \sin 2\psi \\ \sin 2\chi \end{bmatrix} [M] \begin{bmatrix} 1 \\ \cos 2\chi \cos 2\psi \\ \cos 2\chi \sin 2\psi \\ \sin 2\chi \end{bmatrix}^T \quad (20)$$

Where k is the transmitted wavenumber, and T indicates a transpose. The phase angle ψ (0° to 180°) is the orientation angle, and the phase χ is the ellipticity angle ranges from -45° (right_hand circular polarisation) to 45° (left_hand circular polarisation).

A particular graphical representation of the variation of received power as a function of polarisation known as the polarisation signature is quite useful for describing polarisation properties of areas. The signature consists of a plot of synthesised radar cross section as a function of the ellipticity and orientation angles of the transmit antenna. Because the polarisation signature plots capture many scattering characteristics of the target, at all polarisations, the shape of these plots is significant and can indicate the scattering mechanisms dominating the target response.

In all the polarisation signature plots presented, the maximum intensity has been normalised to 1.0. the cross-pol case may be realised by letting the receive antenna ellipticity χ be the negative of the transmit antenna ellipticity and by letting the receive orientation angle ψ be orthogonal to that of the transmit antenna, i.e., $\psi + 90^0$. We illustrate the theoretical signatures of a perfectly conducting dihedral corner reflector (figure 5).

In the dihedral reflector the wave is reflected only twice and as a result the received power for circular polarisations is maximum in the co-polar case, and is zero in the cross-polar case. The co-polarised response passes two minima at linear polarisations offset by +/-45° from the horizontal and vertical polarisations, and the cross-polarised response has maxima at these locations.

The polarisation of a given pixel or region of interest is the sum of the polarisation signatures of many individual scatters.

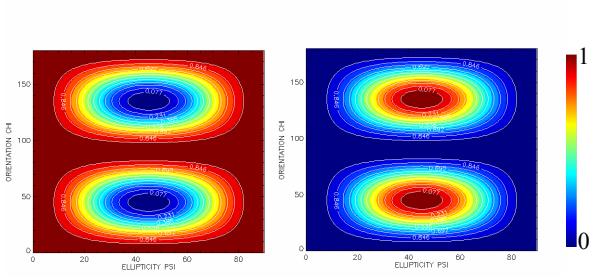

Figure 5: Polarisation responses of a conducting dihedral corner reflector

3.5.2 Polarimetric responses interpretation

In this study, we introduced the shape features of polarisation signature diagram used as a tool for polarimetric SAR data to characterise the forest classes and examining the parameters of the scattering objects.

3.5.2.1 The mixed natural young forest class

Figure 6 shows the polarisation responses of this class. In the co-polar signature, the highest values of intensity are observed for an ellepticity angle at 0°, and an orientation angle at 90° (i.e., vv presents high value). In this case, polarisation is vertically oriented. For the cross-polarised response, the measured intensity has minima at these locations. As a result, the co-polarisation and cross-polarisation plots are characteristic of surface scattering. This occurs because the forest class is young and contains mixed trees with much under growth and with an averaged height of 5m .

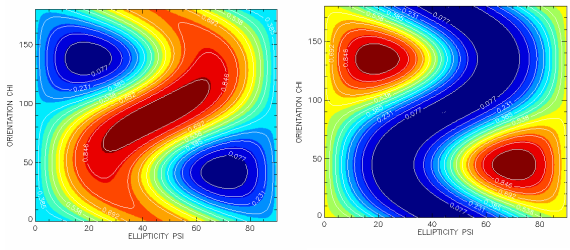

Figure 6 : Polarimetric responses of class1

3.5.2.2 The dense forest class

It can be seen from Figure 7 that the maxima of co-polar signature occurs at the ellipticity angle 0°, and at the orientations angles 0° and 180° (i.e., hh presents high value). This indicates a linear polarisation response, and the targets are horizontally oriented. For the cross-polarised signature, the measured backscattering response has maxima at 45° and 135°. Consequently, the signature denote the contribution of horizontally oriented dipoles (as stems) and multiple scattering due to trunk-ground and branch-branch interactions.

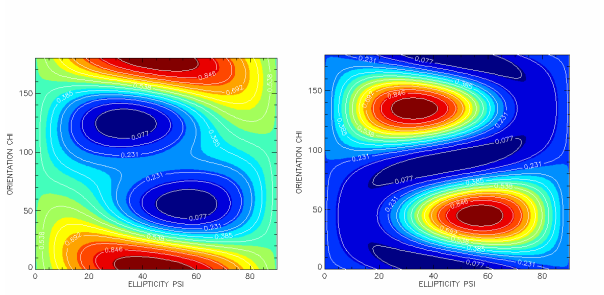

Figure 7 : Polarimetric responses of class 3

3.5.2.3 The old deciduous forest

The forest signature shown in Figure 8 presents high values of co-polar intensity at the ellipticity angle 0° and at orientation angle 0° and 180° (i.e., hh presents high value). This denotes that the highest intensity occurs at linear polarisation and the forest targets are horizontally oriented. This means that this class is dominated by the double bounce scattering from trunk-ground structures.

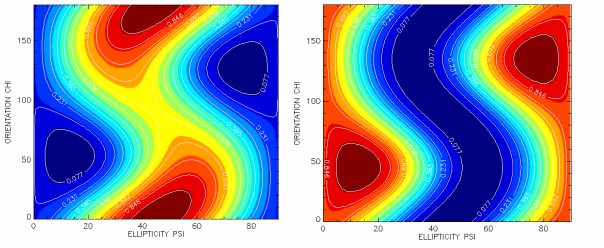

Figure 8 :Polarisation responses of class 3

3.5.2.4 The young deciduous forest

In this class, the polarisation reactions (figure 9) are mainly due to the double bounce reflections from trunk-ground structures, and between the soil surface and the crop canopy. It can be observed that the polarisation responses of this class are almost identical to the second class. The appeared differences are due that this class contains both coniferous and deciduous trees, while the second class contains only coniferous trees. As a result, several secondary scattering mechanisms are produced.

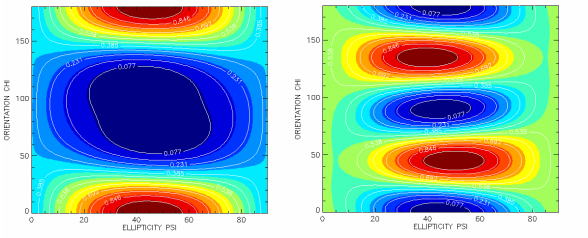

Figure 9: Polarisation responses of class 4

4. CONCLUSION

In this paper, the potential of the polarimetric data to discriminate among different forest classes was investigated, such as extraction of polarimetric signatures, entropy, anisotropy alpha angle, and the combined Wishart classification were used to interpret the scattering mechanisms of each class. We further showed that both the shape of the co-polarisation and cross-polarisation signatures provide information on the dominant scattering mechanism. Given a polarimetric signature, we can extract the scattering parameters such as the type of the polarisation (linear, cicular or elliptical) and the orientation angle at which the target is oriented. From these parameters, we can recognise the scattering behaviour of the forest targets.
Several secondary scattering mechanisms are simultaneously produced, this can make it difficult for the interpreter to distinguish the most characteristic mechanism for the forest class because of the distributed scattering behaviour of the study target.

5. ACKNOWLEDGEMENTS

The Authors wish to thank the Ex company Aerosensing for providing data.

6. REFERENCES

Cloude S. R. and Pottier E., 1996. A review of target decomposition theorems in radar polarimetry. *IEEE transaction on Geoscience and. Remote Sensing*, vol. 34, pp. 498-518

Cloude S. R. and Pottier E., 1997. An entropy based classification scheme for land applications of polarimetric SAR. *IEEE transaction on Geoscience and. Remote Sensing*, vol.35, No. 1, pp 68-78.

Evans . D. L., Farr T. G., Van Zyl J. J. and Zebker H., 1988. Radar Polarimetry: Analysis tools and applications. *IEEE transaction on Geoscience and. Remote Sensing*, vol. 26 no. 6 pp. 774-789.

Freeman A. and Durden S.L., 1998. A three component scattering model for polarimetric SAR data. *IEEE transaction on Geoscience and. Remote Sensing*, vol. 36, no. 3, pp. 963-973.

Lee J. S., Grunes M. R., Ainsworth T. L., Du L. J., Schuler D. L. and Cloude S. R., 1999. Unsupervised Classification using Polarimetric Decomposition and the Complex Wishart Distribution," *IEEE Transactions Geoscience and Remote Sensing,* Vol 37, No. 5, p 2249-2259.

Papathanassiou K. P., 1999. Polarimetric SAR interferometry. *PhD Thesis the faculty of natural sciences, department of physics, technical university Graz*, Austria.

Proisy C., Mougin E., Fromard F., Trichon V. and Karam M. A., 2002. On the influence of canopy structure on the radar backscattering of mangrove forests. *Int. J. of Remote Sensing*, vol. 23, no. 20, pp. 13.

Touzi R. and Chabonneau F., 2002. Characterisation of target symmetric scattering using polarimetric SARs. *IEEE transaction on Geoscience and. Remote Sensing*, vol. 40, no. 11, pp. 693-711.

Ulaby F. T. and Elachi C., 1990. Radar polarimetry for geoscience applications," *Artech House,* Norwood, MA, pp 364.